

## Paper:

# Assimilation Impact of Different GPS Analysis Methods on Precipitation Forecast: A Heavy Rainfall Case Study of Kani City, Gifu Prefecture on July 15, 2010

Shingo Shimizu<sup>\*,†</sup>, Seiichi Shimada<sup>\*\*</sup>, and Kazuhisa Tsuboki<sup>\*\*\*</sup>

<sup>\*</sup>National Research Institute for Earth Science and Disaster Resilience (NIED)

3-1 Tennodai, Tsukuba City, Ibaraki, Japan

<sup>†</sup>Corresponding author, E-mail: shimizus@bosai.go.jp

<sup>\*\*</sup>Graduate School of Frontier Sciences, the University of Tokyo, Tokyo, Japan

<sup>\*\*\*</sup>Institute for Space-Earth Environmental Research, Nagoya University, Nagoya, Japan

[Received April 3, 2017; accepted September 7, 2017]

In this study, we examined variations in predicted precipitable water produced from different Global Positioning System (GPS) zenith delay methods, and assessed the corresponding difference in predicted rainfall after assimilating the obtained precipitable water data. Precipitable water data estimated from the GPS and three-dimensional horizontal wind velocity field derived from the X-band dual polarimetric radar were assimilated in CReSS and rainfall forecast experiments were conducted for the heavy rainfall system in Kani City, Gifu Prefecture on July 15, 2010. In the GPS analysis, a method to simultaneously estimate coordinates and zenith delay, i.e., the simultaneous estimation method, and a method to successively estimate coordinates and zenith delay, i.e., the successive estimation method, were used to estimate precipitable water. The differences generated from using predicted orbit data provided in pseudo-real time from the International GNSS (Global Navigation Satellite System) Service for geodynamics (IGS) versus precise orbit data released after a 10-day delay were examined. The change in precipitable water due to varying the analysis methods was larger than that due to the type of satellite orbit information. In the rainfall forecast experiments, those using the successive estimation method results had a better precision than those using the simultaneous estimation method results. Both methods that included data assimilation had higher rainfall forecast precisions than the forecast precision without precipitable water assimilation. Water vapor obtained from GPS analysis is accepted as important in rainfall forecasting, but the present study showed additional improvements can be attained from incorporating a zenith delay analysis method.

**Keywords:** GPS precipitable water, data assimilation, precipitation forecast

## 1. Introduction

Water vapor content is one of the most important variables in rainfall forecasting [1]. To improve rainfall forecasts, data assimilation methods using precipitable water estimated from the delay in radio wave propagation from Global Positioning Systems (GPS), termed GPS precipitable water, has been developed [1–6]. GPS observations have a higher time-space resolution than sonde observations and can provide significant continuous water vapor content measurements over a wide area. In Japan, the GPS Earth Observation Network (GEONET) was developed by the Geospatial Information Authority of Japan to provide the precipitable water distribution for  $\geq 1200$  locations throughout the country.

The precision of precipitable water observations using GPS zenith delay have been compared with sonde observations. The reported root-mean-square error of the precipitable water measured using GPS zenith delay was 3.37 mm or smaller in summer and 1.64 mm or smaller in winter [5]. Better estimation precision is needed for summer because local severe rain or localized heavy rain is both common and dangerous. Recently, new attempts on multidirectional extraction of water vapor data from GPS data have been made. For example, in addition to zenith delay, the delay in slant path has been used to estimate the horizontal distribution of water vapor [7–8] for data assimilation [9]. The direct assimilation of delay in slant path has two advantages. (1) Unlike zenith delay, which is obtained as a mean delay of signals from multiple GPS satellites directly above the GPS observation point, signals from individual GPS satellites can be directly used. (2) The horizontal gradient of water vapor can be obtained using satellites located at a low elevation angle. However, the large computational cost due to calculating the propagation path of each radio wave signal is a drawback. In this study, we estimated water vapor using the zenith delay because water vapor field at the mesoscale, i.e., several hundred km, needs to be analyzed on the basis of GPS network with several hundreds of observation points.

The primary objective of the present study was to im-



prove the precision of zenith delay estimations and provide a corresponding better precision in precipitable water estimates. Various causes for estimation errors in the zenith delay were comprehensively studied in Ref. [10]. In this study, we focus on the uncertainty caused by rounding the phase bias to integer values. The aim of the GPS observation is to determine the position of a receiver based on the distance between the GPS satellite and receiver. Here, we briefly discuss this issue for simplicity, but equations and details can be found in Ref. [11]. The coordinates ( $X, Y, Z$ ) and time error of the receiver are all unknown values. Therefore, distances to at least four satellites are needed to mathematically determine unknown values. If more than four satellites are available, unknown values are determined by the least squares method, which also accounts for the measurement error. The distance to a satellite is measured by counting the wave number of the propagating wave. However, because phase information is used in the actual measurement, uncertainties in the integer multiples of the wave number remain. The distance can be obtained if this integer can be determined. The distance, i.e., the coordinates, can be identified by appropriately determining the integer value using the least squares method when there is a lack of error factors, such as atmospheric delay. However, because the atmospheric delay is also an unknown value, the unknown values of the delay and coordinates are all simultaneously determined in most cases. In this study, the simultaneous estimation of the delay and coordinates is called simultaneous estimation method. In this method, there is a trade-off between the estimation precision of the delay and coordinates, and the estimation error of the delay may contain the estimation error of the coordinates. This problem can be addressed using the successive estimation method [12]. The coordinates, with a more accurate estimation, are first fixed using the least squares method to reduce the number of unknown values, and then the zenith delay can be determined accurately. Using this method in Ref. [12], the delay was estimated after the coordinates were accurately determined from GPS information from the prior 30 days. Although the 30-day data contain various error factors related to the air field, they were cancelled out by taking an average. Because Ref. [10] reported that the time variation scale of the delay is smaller than that of the coordinates, we can expect the errors to cancel each other in the averaging operation.

As stated above, the estimation of precipitable water could change depending on the estimation method for zenith delay. In this study, we compared the precipitable water obtained from the successive estimation method proposed in Ref. [12] and the conventional simultaneous estimation method. We examined the resulting difference in water vapor distribution and the influence on assimilation experiments.

As a case study, we evaluated the heavy rainfall that occurred in Kani City, Gifu Prefecture on July 15, 2010 (hereinafter referred to as Kani Heavy Rainfall). The damage caused by the Kani Heavy Rainfall has been reported in Refs. [13] and [14], and the meteorological

mechanism was clarified in Ref. [15]. Here, we summarize these studies. After July 11, 2010, warm and wet air moved into Gifu Prefecture and around toward a low pressure area and front moving northeast over the Japan Sea. The warm and wet air caused intermittent rainfall. In the evening of July 15, the rainfall changed to heavy rain in the Kani River valley. At Mitake observatory, one-hour precipitation from 6 PM to 7 PM Japan Standard Time (JST) reached 76 mm, the maximum in observation history at the site, and 3-h precipitation from 5 PM to 8 PM reached 196 mm. The water level at the Tsuchida Water Level Observatory suddenly increased 1 m in the period from 7 PM to 8 PM, and reached a maximum level of 4.25 m at around 8:30 PM [13]. There were overtopping flows in Dota District and Hiromi District in Kani City, and a landslide in Nogami District in Yaotsu-cho resulted in 6 dead or missing people. According to Ref. [15], an air current of high equivalent potential temperature continuously moved in from the southwest at an altitude lower than 2 km in the time period between 6 PM and 8 PM, which constantly formed an updraft without settling the atmospheric instability. The echo top height of the cumulonimbus was maintained at 15 km for an extended period of time. When the cumulonimbus disappeared, a strong downdraft formed and a cold outflow in the southwest direction (northeast current) developed near the ground. The northeast current from the cumulonimbus drew in a warm and wet current from the southwest at almost the same place, forming an updraft, which then formed a new cumulonimbus continuously around Kani City. Reference [15] explained the development of heavy rainfall based on the continuous formation of a strong updraft in the same place.

In Section 2, we describe GPS data and radar data used in the present study and provide an overview of the radar analysis method, numerical model, and numerical experiment. In Section 3, we show the difference in the precipitable water between types of GPS analyses. In addition, we show a time change in the wind velocity field in the radar observations used in the data assimilation. We also compare the observation result and the rainfall distribution obtained in the forecast experiments using data assimilation. In Section 4, we summarize the study and highlight future problems that should be addressed.

## 2. Data and Analysis Method

This study describes differences in the analysis methods for the zenith delay using GPS, and associated differences in assimilation impacts on rainfall forecasts. In this section, we show an overview of the GPS and radar data used in the data assimilation and explain a numerical model and results of a numerical experiment.

### 2.1. GPS Analysis

**Figure 1** shows the GEONET observation points. We chose ~470 GPS observation sites in and around Chukyo

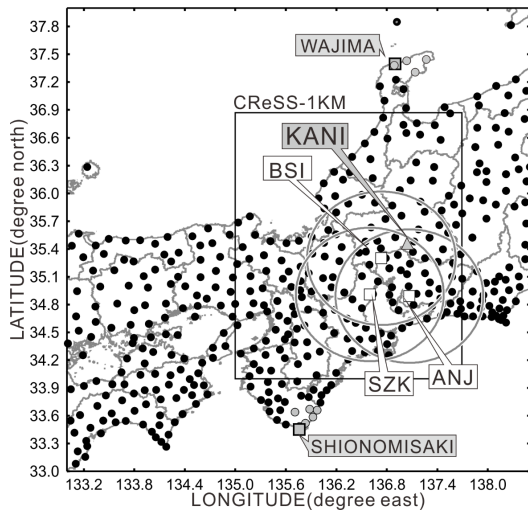


**Fig. 1.** GPS observation points and radar observation areas (gray circles) from the Ministry of Land, Infrastructure and Transport for Anjo City (ANJ), Bisai City (BSI), and Suzuka City (SZK) in the GEONET observation network. The calculation area for the numerical experiment, CReSS-1km, is also shown. Sonde observations were collected at Shionomisaki and Wajima (gray square). The precipitable water average over the GPS observation points indicated with gray circles was compared with observation data from the sonde. The location of Kani City, where heavy rainfall was observed, is indicated with a gray triangle.

District, where the Kani Heavy Rainfall occurred, to study differences in precipitable water. In addition, the obtained precipitable water data were used for data assimilation. The computational area of the numerical simulation with data assimilation is shown in **Fig. 1**. The locations of Shionomisaki and Wajima, where sonde observations are currently collected by the Japan Meteorological Agency (JMA), are presented in **Fig. 1**.

The GPS analysis software programs GAMIT and GLOBK [16–17], hereinafter referred to as GAMIT software, were used. We omit explanation of the simultaneous estimation method, as it is thoroughly explained in Refs. [17–18]. In the simultaneous estimation, we used the predicted orbit data, transmitted in pseudo-real time, as satellite orbit information. In contrast, we used the precise orbit data in the successive estimation and performed the analyses according to the method described in Ref. [12]. We summarize the method in the following three steps.

- (1) The GAMIT program estimates the coordinates every day over 30 days using the strong constraint of the IGS coordinate reference point.
- (2) The GLOBK program determines a single set of highly accurate coordinates based on error information and the coordinates estimated every day using a Kalman filter.
- (3) The obtained highly accurate coordinates are used to obtain the zenith delay. The time resolution of the zenith delay was set to 1 h.

**Table 1.** Difference in GPS data used in this study.

Data name	GPS1	GPS2	GSI
Method	Successive estimation method	Simultaneous estimation method	Simultaneous estimation method
Satellite orbit information	Precise orbit	Predicted orbit	Precise orbit
Time resolution	1 hour	1 hour	3 hours

The conversion from the zenith delay to precipitable water was made according to the methods provided in Ref. [19]. Ground air pressure and temperature at GPS observation points used in the estimation of zenith hydrostatic delay were obtained from the numerical results of the meteorological model CReSS, described in Section 2.3, without data assimilation. Only the GPS observation points within 500 m of the elevation used in the numerical experiment were used for analysis and data assimilation.

In this study, we conducted analysis based on GAMIT software and also used, as reference data, the F3 solution [20] product provided by the Geospatial Information Authority of Japan. The F3 solution from the Geospatial Information Authority of Japan, hereinafter referred to as GSI product (“GSI” is old acronym of Geospatial Information Authority of Japan), has a time resolution of 3 h. GSI conducts analysis using Bernese software and employs the simultaneous estimation method with precise orbit data. **Table 1** summarizes the difference in these three GPS data sources.

## 2.2. Observation Data and Radar Analysis

**Figure 1** shows the observation area for the X-band radar operated by the Ministry of Land, Infrastructure and Transport (MLIT). Reflectivity and radial velocity obtained from the MLIT X-band radars, termed XRAIN, located in Anjo City, Bisai City, and Suzuka City were used to conduct a three-dimensional variational analysis [21] of wind, and horizontal wind components in the rainfall system were used for data assimilation. The radar data specifications are provided in **Table 1** in Ref. [15]. Details of the analysis method are identical to those in Ref. [15]. The mesh resolution was 1 km in the horizontal direction and 250 m in the vertical direction. The analysis volume was 480 × 480 km wide and 12 km high. In the three-dimensional radar analysis, the estimation precision for the horizontal wind velocity is usually higher than that for the vertical wind velocity [22], hence only horizontal wind was used in the data assimilation in the present study.

Rainfall data from radar-AMeDAS precipitation analysis from JMA were used. Every 30 min, radar-AMeDAS provides accumulated rainfall for the prior hour. Therefore we used 1-h accumulated rainfall from the radar-AMeDAS precipitation analysis and 6-h accumulated rainfall for the period from 06:00 to 12:00 UTC (Coordi-

nated Universal Time; Japan Standard Time is +9 h from UTC) on July 15, 2010. The radar-AMeDAS precipitation analysis provides precipitation data covering the entire country with a mesh resolution of 1 km.

To analyze the meteorological fields, water vapor mixing ratios obtained every 10 min from operational ground observations and air temperature measured every 10 min by AMeDAS were used. Only data from observation sites at elevations of  $\leq 150$  m were used to analyze the horizontal distribution of the obtained data. Assuming a typical temperature lapse rate, i.e.,  $6^{\circ}\text{C}$  per 1000 m, the temperature difference due to the elevation differences could be suppressed to  $\leq 1^{\circ}\text{C}$ . Therefore, the estimation error for water vapor due to elevation differences also expected to be small.

### 2.3. Overview of Numerical Model and Numerical Experiment

We used a cloud resolving numerical model CReSS [23] for rainfall forecasting. An overview of the numerical model is provided in **Table 1** of Ref. [24], and we performed the experiment using the same scheme. The mesh resolution is 1 km in the horizontal direction and variable in the vertical direction. The vertical mesh resolution is 100 m in the lower layer and becomes coarser with elevation for an average vertical resolution set to 300 m. At the top of the model calculation volume, the elevation and pressure are set to 20.8 km and 54 hPa, respectively. The calculation volume shown in **Fig. 1** contains 300 points  $\times$  320 points  $\times$  70 layers. The forecast calculation was performed from 06:00 to 12:00 UTC on July 15, 2010. Output from the Mesoscale Model (MSM) [25–27] of the JMA was used for initial values and boundary values. For the lateral boundary condition, predicted values every 3 h from the MSM were used. Elevation data were based on the global digital elevation model GTOPO30, provided by the United States Geological Survey (USGS). Land use data were generated from the Global Land Cover Characterization (GLCC) provided by the USGS. Sea surface temperature data were generated from merged satellite and *in situ* data global daily sea surface temperature (MGDSST) provided by the JMA [27–28].

We conducted a control experiment without data assimilation, hereinafter referred to as the CNTL experiment, and output calculation results every 5 min. Using the ground atmospheric temperature and pressure from the CNTL experiment, we converted the zenith delay data to precipitable water data for all GPS products.

The following four different experiments with data assimilation were conducted.

- (1) Assimilation and forecast experiments for precipitable water obtained from the successive estimation method, referred to as the GPS1 experiments.
- (2) Assimilation and forecast experiments for precipitable water obtained from the simultaneous estimation method, referred to as the GPS2 experiments.

- (3) Experiments incorporating the nudging assimilation of radar horizontal wind data with GPS1, referred to as the GPS1+UV experiments.
- (4) Experiments incorporating the nudging assimilation of radar horizontal wind data with GPS2, referred to as the GPS2+UV experiment.

The assimilation time was set to 3 h, from 06:00 to 09:00 UTC, and the precision of the rainfall forecast for the 6 h from 06:00 to 12:00 UTC was assessed. The GPS data were assimilated every 1 h and the radar data were assimilated every 5 min. The assimilation windows for the GPS and radar data were set to 30 min and 2.5 min before and after the observation time, respectively. For the data assimilation of precipitable water, a method that combines three-dimensional variational method (3DVAR; [29]) and incremental analysis update filter (IAU; [30]) was employed (3DVAR+IAU; [31]). A simple nudging method [32] was employed for radar data assimilation.

## 3. Results

In this section, we show variations in the precipitable water due to differences in the GPS analyses, and the corresponding variations in forecast results with the assimilated precipitable water data.

### 3.1. Comparison of GPS Analyses

**Figure 2** shows the precipitable water distributions every 3 h obtained using the different GPS analyses. There is no significant difference in the distributions between GPS2 and GSI. In contrast, the area north of  $35^{\circ}\text{N}$  at 03:00 UTC before the rainfall is drier in GPS1 than in GPS2. The dry air in the northern area remains at 09:00 UTC when the rainfall begins. In the GPS2 panel, the north-south gradient gradually decreases as time passes from 03:00 to 09:00 UTC. Both sets of GPS data indicate the presence of wet air in the Mie, Nara, and Wakayama Prefectures on the windward side of Kani City, Gifu Prefecture, where the heavy rainfall occurred. Only the GPS1 data indicated the presence of a large north-south gradient in water vapor around  $35^{\circ}\text{N}$ .

This north-south gradient in precipitable water around  $35^{\circ}\text{N}$  is also shown in the water vapor observation data from the ground (left in **Fig. 3**). At 03:00 UTC, the difference in the ground water vapor mixing ratio is about 3–5 g/kg, and the north-south gradient in the ground water vapor mixing ratio around  $35^{\circ}\text{N}$  decreased between 06:00 and 09:00 UTC. In the GPS1 panel in **Fig. 2**, the variations in the north-south gradient of the precipitable water around  $35^{\circ}\text{N}$  with time is in good agreement with the ground water vapor mixing ratio, although the comparison between ground vapor and vertically integrated vapor is rather indirect. In contrast, the north-south gradient in temperature around  $35^{\circ}\text{N}$  (right in **Fig. 3**) was not significant at 03:00 or 06:00 UTC. The temperature was

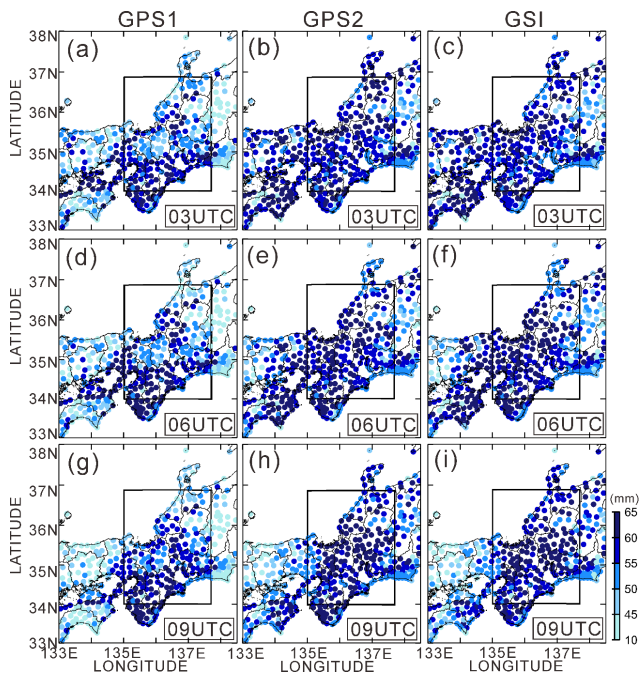


**Fig. 2.** Temporal evolution of GPS precipitable water distribution on July 5, 2010. Data from the upper, middle, and lower row panels show the data at 03:00, 06:00, and 09:00 UTC, respectively. The left, middle, and right column panels show the data obtained from GPS1, GPS2, and GSI, respectively. The squares indicate the numerical calculation areas.

uniform around 35°N at 09:00 UTC. The north-south gradient in the water vapor mixing ratio around 35°N may correspond to a shear line in the wind vector between the southwest and south wind in the 950 hPa analysis data shown in Fig. 21a of Ref. [15].

To quantitatively examine the difference in the discussed water vapor distributions, the average and standard deviations were calculated at the GPS observation points in the numerical calculation area, and are shown in Fig. 4 as a box plot. The average for GPS1 is smaller than those for GPS2 or GSI at any time in the entire calculation area, although the standard deviation for GPS1 is larger. For calculations limited to the south side of 35°N, the average for GPS1 is larger than those for GPS2 or GSI at any time. Therefore, the results in Figs. 2 and 4 indicate that, compared to GPS2 or GSI, GPS1 tends to show drier air on the north side of 35°N and wetter air on the south side. Fig. 5 shows a scatter diagram of precipitable water at the observation points. The horizontal and vertical axes show different data types to evaluate the similarity in the data. The GSI and GPS2 data have an extremely high correlation and small bias, while the GPS1 and GPS2 data have a relatively high correlation but the GPS1 data have a negative bias, ~4.7 mm.

The GPS observation results are compared with data obtained from the sonde measurements, which are independent of GPS observations. The sonde data from Shionomisaki, Wakayama Prefecture and Wajima, Ishikawa Prefecture (Fig. 2) at 12:00 UTC were used. Measurements from Shionomisaki indicates precipitable water of

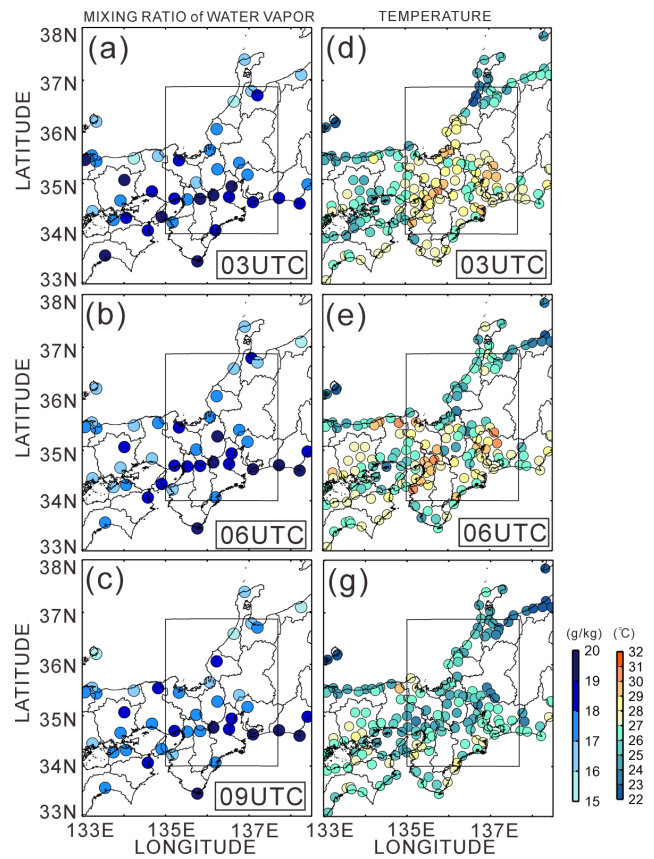


**Fig. 3.** Temporal evolution of Ground observation data from the Japan Meteorological Agency on July 5, 2010. Left panels are ground water vapor mixing ratios and right panels are AMeDAS atmospheric temperatures. As in Fig. 2, the squares indicate the numerical calculation areas. Only the data at the observation sites with elevations of <150 m are shown.

55.21 mm, while those from Wajima indicates precipitable water of 51.30 mm. The spatial density of the sonde data is much smaller than that of the GPS observations; nonetheless, a comparison of sonde data between Shionomisaki and Wajima indicates that the precipitable water at Shionomisaki, located south of Wajima, is ~4 mm higher. The sonde data also indicate that the maximum wind velocity at an elevation of  $\leq 10$  km was 15 m/s, and from the southwest (figure omitted). Assuming that the upward speed of sonde has a typical speed of 5 m/s, it would reach an elevation of 10 km in 2000 seconds. This suggests that the sonde observed an area about 30 km away in the northeast direction from the point the sonde was released. Therefore, we calculated average GPS precipitable water over a 30 km square lying on the northeast side of Shionomisaki or Wajima, with the southwest corner of the square fixed on Shionomisaki or Wajima, and compared it with the precipitable water obtained from sonde observations. In the average calculation, data from the observation points indicated with gray circles in Fig. 1 were used. The precipitable water near Shionomisaki at 12:00 UTC was 55.59, 54.64, and 54.74 mm, respectively for GPS1, GPS2, and GSI. The differences from the observation data were +0.38 mm,

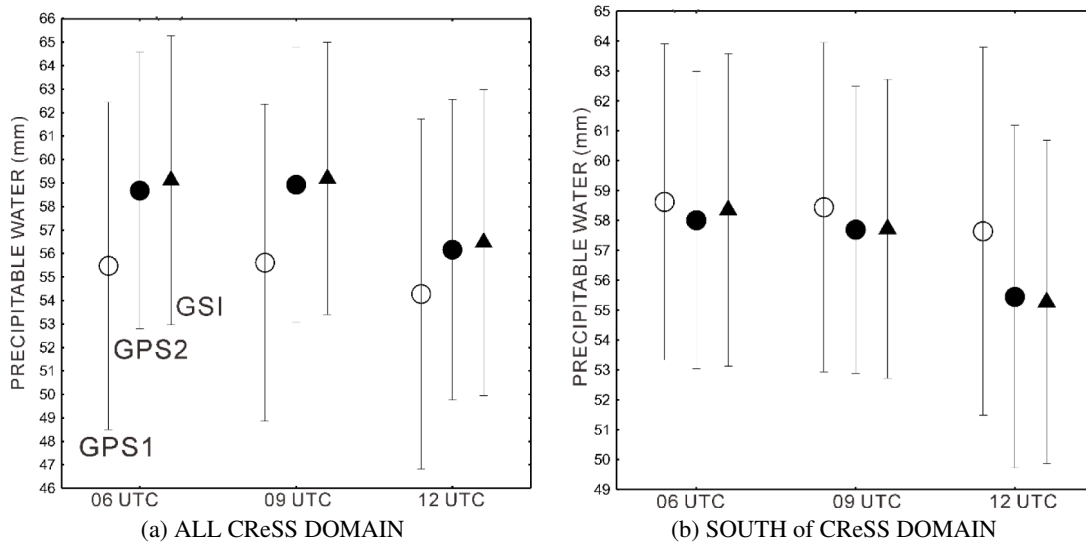


**Fig. 4.** Average and standard deviation of GPS precipitable water for each time. The left shows the data for the entire numerical calculation area in **Fig. 2**. The right shows data for an area south of 35° N in the numerical calculation area.

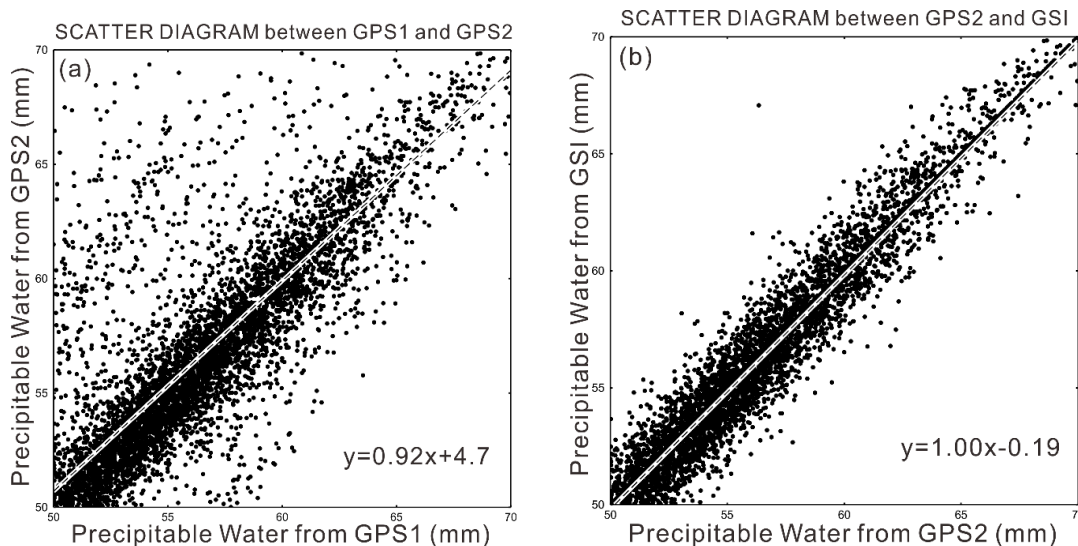


**Fig. 5.** Scatter diagram of precipitable water from the three GPS systems. The *x*-axis for the left panel is data from GPS1 and the *y*-axis is data from GPS2. The *x*-axis for the right panel is data from GPS2 and the *y*-axis is data from GSI.

−0.57 mm, and −0.47 mm, respectively, indicating similarity in the three estimation methods. The data from GPS1 provided the closest result to the observation result. In contrast, the precipitable water near Wajima was 45.61, 52.7, and 52.88 mm, respectively for GPS1, GPS2, and GSI. The differences from the observation data were −5.61 mm, +0.95 mm, and +1.59 mm, respectively, which indicates an extremely large negative bias in the data for GPS1 and positive bias for GPS2 and GSI. Assuming that the precipitable water data from the sondes at Wajima and Shionomisaki are accurate, the GPS1 data has a larger north-south gradient in the water vapor mixing ratio and GPS2 and GSI data have a smaller north-south gradient.

Based on the data and discussion, there was no significant difference in the precipitable water between GPS2 and GSI. GPS2 and GSI use the same simultane-

ous estimation method, but they use different satellite orbit information, orbit precision, and predicted orbit. The present study shows that the difference in the analysis method has a larger influence on the estimation of precipitable water than differences in satellite orbit information. Based on these results, we hypothesize that the precision of the precipitable water estimation using a precise orbit is almost identical to that using a predicted orbit. Therefore, we focus on the difference in the estimation methods in the following discussion. The validity of this assumption will be discussed elsewhere. Now we compare the forecast experiments using GPS2 and GPS1, which have high time resolutions.

### 3.2. Results of Radar Analysis

**Figure 6** shows a distribution of radar-AMeDAS anal-

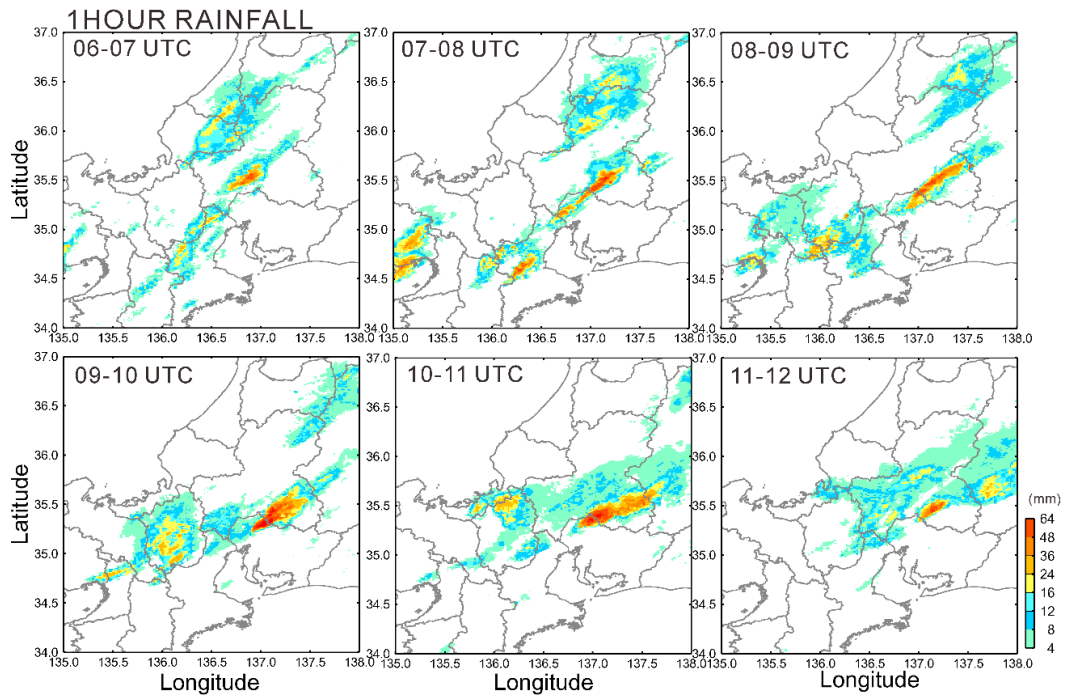


**Fig. 6.** Distribution of 1-h accumulated rainfall from radar-AMeDAS analysis. The time range used for the calculation of accumulated rainfall is shown in the upper left corner of each panel.

ysis rainfall. In Kani City, located at the border between Aichi and Gifu Prefectures, heavy rainfall continued after 06:00 UTC on July 5, 2010. The radar-AMeDAS analysis showed that accumulated rainfall in the hour between 09:00 and 10:00 UTC reached 95 mm. This continued heavy rainfall in a relatively small area could have caused the significant damage [13]. The formation mechanism for the heavy rainfall has been studied in detail in Ref. [15]. Reference [15] concluded that the wind convergence around an elevation of 1.5 km continued from 07:00 to 09:00 UTC, which resulted in heavy, stationary, and continuous rainfall for an extended period of time (Fig. 9 of Ref. [15]). In the present study, the wind velocity field (Fig. 7) from 06:00 UTC, when the rainfall began, to 09:00 UTC was used to assimilate the convergence of the lower wind. Reference [15] provides a wind velocity field averaged over 3 h. In Fig. 7, we show the wind velocity field for every hour at an elevation of 1.0 km. Overall wind in the velocity field is southwest, but convergence of a south wind on the south side of the rainfall area and a southwest wind on the west side was observed in the heavy rainfall area at 07:00 and 08:00 UTC. Because the convergence occurred locally, the wind data assimilation should contribute to the reproduction of locally occurring rainfall.

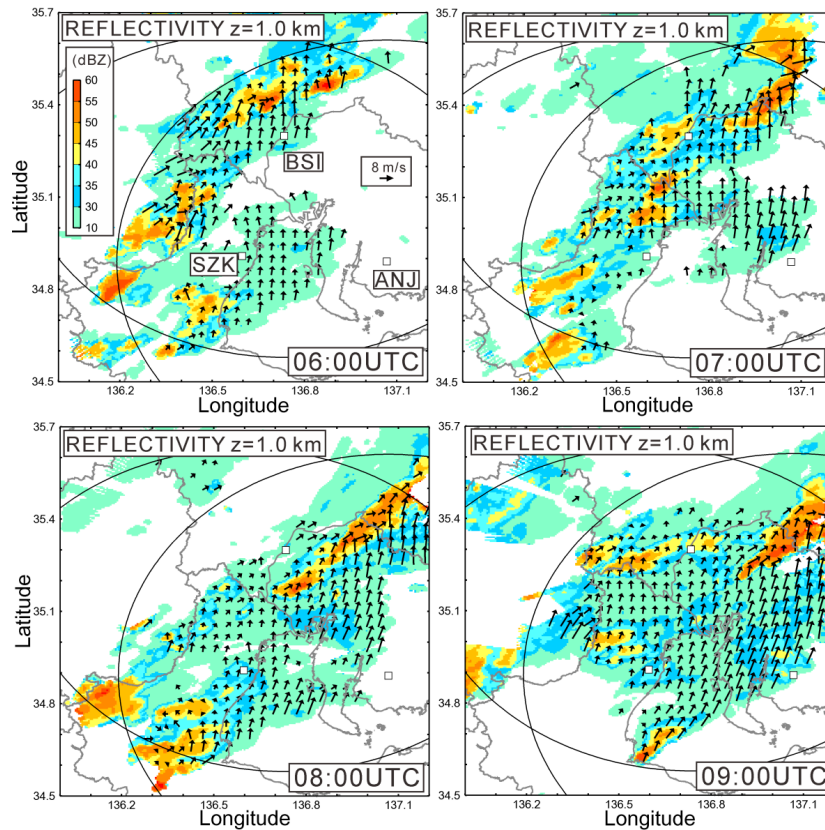
### 3.3. Assimilation Experiment Results

We compared the distribution of the 6-h accumulated rainfall with the observation results and examined the experiment performances in quantitatively reproducing the observed rainfall distribution. We also evaluated the accuracy of the numerical experiments in reproducing the ob-

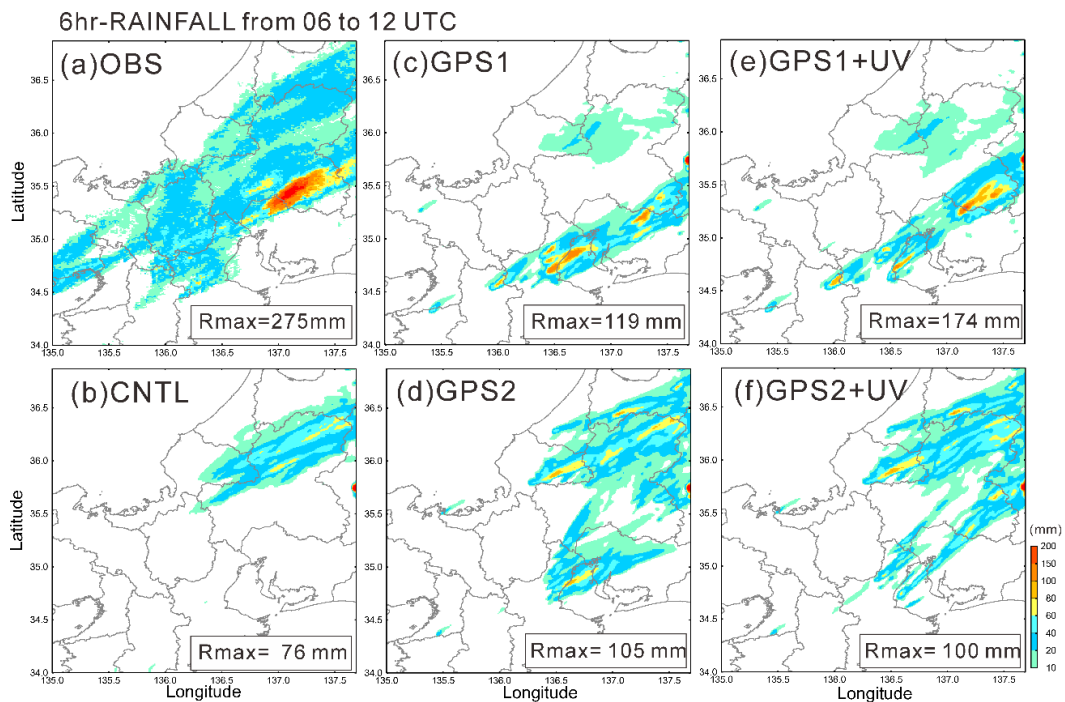
served maximum rainfall; the reproducibility of the continued heavy rainfall was verified by examining the variation in the maximum 1-h accumulated rainfall over time. The present study investigated the influence of data assimilation in different GPS methods, and the grid-to-grid evaluation of precision is left for future work.

Figure 8 shows the observed and experimentally predicted 6-h accumulated rainfall. In the observation, rainfall higher >100 mm was recorded in a narrow area, 60 × 50 km. The maximum rainfall was 275 mm. The 6-h accumulated rainfall was relatively low, ≤40 mm, in many other places.

In the CNTL experiment with no data assimilation, heavy rainfall exceeding 100 mm was not reproduced, and the maximum rainfall occurred in northern Gifu Prefecture. The rainfall in southern Gifu was not reproduced at all. The result could not be improved even using initial values obtained from the Japan Meteorological Agency Mesoscale Analysis (JMA-MA) instead of the MSM (figure omitted). JMA-MA is the analysis to produce initial condition of JMA-MSM. The GPS precipitable water is also assimilated in the JMA-MA. However, their mesh resolution is set to 15 km to lower the computational cost, and GPS observation data were discarded every 30 km in data assimilation procedure [33]. Therefore, the gradient in the water vapor mixing ratio around 35°N might not have been sufficiently taken into account. The rainfall at 35.7°N and 137.7°E degrees simulated in every forecast experiment was due to a spurious updraft near the lateral boundary of the numerical calculation volume. This spurious updraft was on the lee side of southern Gifu, our study target, and should not have affected the calculation results.



**Fig. 7.** Reflectivity intensity at an elevation of 1.0 km and distribution of horizontal wind obtained from three-dimensional wind velocity analysis.



**Fig. 8.** Distribution of 6-h accumulated rainfall. The upper left panel is radar-AMeDAS analysis rainfall data from 06: 00 to 12:00 UTC. The lower left panel presents the results from the CNTL experiment. The middle column shows results from the GPS1 (top) and GPS2 (bottom) experiments. The right column shows the results from the GPS1+UV (top) and GPS2+UV (bottom) experiments, wherein both precipitable water and radar wind were assimilated. The maximum rainfall is indicated in the lower right corner of each figure.

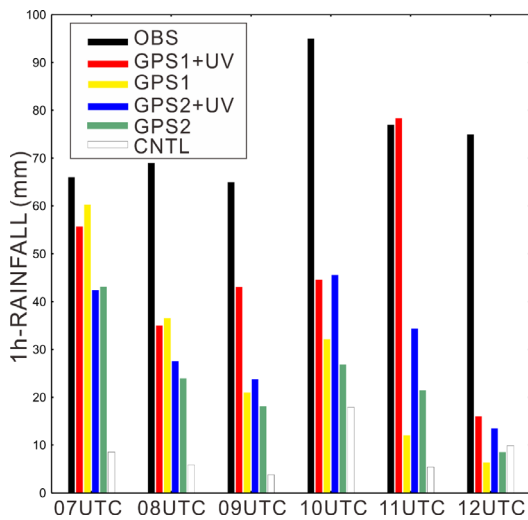


**Fig. 9.** Variation in the maximum 1-h accumulated rainfall in and around Kani City measured over a 5 h period. The horizontal axis shows the end of accumulation time, e.g., the bars at 07:00 UTC show the 1-h accumulated rainfall measured from 06:00 to 07:00 UTC in the 60 × 50 km area in and around Kani City. OBS indicates the rainfall obtained from the radar-AMeDAS analysis rainfall data. CNTL, GPS1, GPS2, GPS1+UV, and GPS2+UV indicate the rainfall obtained from the experiments described in the text.

Unlike CNTL experiment, the GPS1 and GPS2 experiments successfully reproduced the rainfall in southern Gifu Prefecture. The GPS1 experiment had weaker rainfall in northern Gifu and stronger rainfall in southern Gifu than in the CNTL experiment. The GPS1 experiment reproduced the heavy rainfall, >100 mm, in the area about 40 km east of Kani City. It also reproduced the heavy rainfall in Ise Bay. The observed rainband extending from the southwest to northeast was reproduced in the GPS1 experiment, but was located about 30 km south of the observed location. The GPS2 experiment showed an intermediate result between the CNTL experiment and GPS1 experiment. It incorrectly reproduced the heavy rainfall in northern Gifu, and the rainfall was higher than in the CNTL experiment. The heavy rainfall >100 mm was incorrectly reproduced in Fukui Prefecture.

Finally, we examined GPS1+UV and GPS2+UV experiments where the radar wind was assimilated. Compared to the GPS1 experiment, the GPS1+UV experiment resulted in a lower rainfall in Ise Bay and a higher rainfall on the border between Aichi and Gifu Prefectures. The rainfall on the border between Aichi and Gifu Prefectures forecasted in the GPS1+UV experiment was most similar to observed rainfall. The maximum rainfall in the GPS1+UV experiment was 174 mm. This is not as high as the observed maximum rainfall of 275 mm, but higher than the maximum rainfall in all other experiments. The GPS2+UV experiment produced a lower rainfall in Ise Bay, higher rainfall on the border between Aichi and Gifu Prefectures, and maximum rainfall in Fukui Prefecture.

Around the border between Aichi and Gifu Prefectures, a 60 × 50 km area, corresponding to the area where ob-

served 6-h accumulated rainfall reached ≥ 100 mm and centered on the site where a maximum rainfall of 275 mm was observed, was chosen and the temporal variation in maximum 1-h accumulated rainfall is shown in **Fig. 9**. The observed maximum 1-h accumulated rainfall data indicate that the heavy rainfall, >60 mm, continued anywhere in and around Kani City throughout the time period from 07:00 to 12:00 UTC. The CNTL experiment failed to reproduce rainfall of >20 mm at any time. All other experiments, GPS1, GPS2, GPS1+UV, and GPS2+UV, with assimilated GPS precipitable water data, produced higher 1-h accumulated rainfall than the CNTL experiment in all hours except 12:00 UTC. The experiments with assimilated GPS precipitable water and radar wind, GPS1+UV and GPS2+UV, produced higher rainfall than the CNTL experiment for all hours. This suggests that the GPS data assimilation experiments can improve rainfall forecasting, in agreement with previous studies.

Comparing the GPS1 and GPS2 experiments, the GPS1 experiment forecasted a higher rainfall from 07:00 through 09:00 UTC, when data assimilation was performed. At 10:00 UTC, after 1 h from the end of assimilation window (06:00-09:00 UTC), the GPS1 experiment still forecasted a higher rainfall than the GPS2 experiment. However, at 11:00 and 12:00 UTC, the superiority of the GPS1 experiment over the GPS2 experiment disappeared. Therefore, the superiority of the GPS1 experiment continued for about an hour after data assimilation ended.

Comparing the GPS1 and GPS1+UV experiments, no significant difference was observed in the period from 07:00 to 08:00 UTC, during data assimilation, but the advantage of the GPS1+UV experiment was confirmed in the period from 09:00 to 12:00 UTC; the GPS2 and GPS2+UV experiments behaved similarly. This observation suggests that the wind velocity field was important for reproducing the continued local heavy rainfall.

#### 4. Discussions and Conclusions

In this study, we examined the variations in predicted precipitable water due to differences in GPS zenith delay analysis methods. We then evaluated the corresponding differences in predicted rainfall after assimilating the precipitable water data. For the heavy rainfall system in Kani City, Gifu Prefecture on July 15, 2010, the precipitable water estimated from GPS data and three-dimensional horizontal wind fields obtained from the X-band dual polarimetric radar were assimilated in CReSS, and rainfall forecasting experiments were conducted. In the GPS analyses, a method to simultaneously estimate coordinates and zenith delay, i.e. the simultaneous estimation method, and a method to successively estimate coordinates and zenith delay, i.e., the successive estimation method, were used to estimate precipitable water. To determine the contribution from the GPS satellite orbit information used in the zenith delay calculations, differences between results from the predicted orbit provided in pseudo-real time and

precise orbit released 10 days later were evaluated. We found that the difference in analysis method was more important than satellite orbit information in predicting precipitable water. The successive estimation method produced a large difference in water vapor between southern Gifu, where the heavy rainfall was observed, and the northern Gifu. In comparison, the simultaneous estimation method did not show a water vapor gradient between the northern and southern areas.

In the rainfall forecast experiments, the successive estimation method produced better result in the 6-h accumulated rainfall distribution than the simultaneous estimation method. The experiment with assimilated precipitable water data from the successive estimation reproduced the rainband in southern Gifu and the rainfall area in northern Gifu that were forecast in the control experiment (no data assimilation experiment). Compared with the control experiment, the experiments with data assimilation more precisely forecasted rainfall up to 5 hours after initial time of numerical simulation (including 3 hours of assimilation window period).

Assimilation of both GPS water vapor information and radar wind data significantly contributed to reproducing the observed continued heavy rainfall. Without radar wind data assimilation, the forecast precision was significantly worse about an hour after data assimilation ceased. In contrast, with radar wind data assimilation, heavy rainfall could be reproduced even 2 h after data assimilation ceased. Three hours after data assimilation ceased, all experiments produced similar results, regardless of radar wind assimilation.

The amount of water vapor from GPS analyses have been accepted as important for rainfall forecasting, but the present study showed that the zenith delay analysis method can significantly improve forecasting. The improvement in precipitable water and rainfall forecasting due to choosing an appropriate GPS analysis method indicates can also contribute to forecasting rainfall several hours in advance. However, to show the generality of these results, the following two issues need to be statistically investigated. First, superiority of the successive estimation shown in this study needs to be evaluated for both locally severe rain or other extreme weather events and also for times with little or no precipitation. Second, the possibility that the appropriate choice of the magnitude in GPS position variation error in the simultaneous estimation method could improve the precipitable water estimation needs to be verified for large water vapor fluctuations during extreme weather events. In the present study, we examined forecast results with a focus on the reproducibility of maximum rainfall; examining forecasts of other weather factors remains a future problem. In addition, relatively simple data assimilation methods, such as 3DVAR and nudging, were employed in this study and more advanced data assimilation methods, such as 4DVAR or ensemble Kalman filter, could be used. The potential improvements from applying these methods remains to be investigated. Furthermore, while radar wind and retrieved precipitable water were incorporated in the

prediction methods in this study, the influence of incorporating other observation data on the model results should also be examined.

In the future, water vapor analysis methods can be made more universal by applying them to additional case study examples and evaluating statistically-significant improvements in the rainfall forecasts. Errors in forecasts using data assimilation can be evaluated by performing statistical analyses on forecast experiments with the GPS analysis method proposed in the present study. In addition, by investigating the precision of estimations using the predicted orbit and successive estimation method, the influence of precipitable water data assimilation can be evaluated in real time to examine the usability for weather forecasting.

### Acknowledgements

The XRAIN data used in the study were provided by the Ministry of Land, Infrastructure and Transport. The data set was collected from or provided under the framework of the National Key Technology "Marine earth observation exploratory system": Data Integration and Analysis System (DIAS), Data Integration and Analysis System Program (DIAS-P), and Global Environment Information Platform Development Promotion Program. The GPS data were obtained from the Geospatial Information Authority of Japan. The analysis tool provided by Yusuke Morimoto, Graduate School of Environmental Studies, Nagoya University was used for data processing the F3 solution from the Geospatial Information Authority of Japan.

### References:

- [1] Y. H. Kuo, X. Zou, and Y.R. Guo, "Variational assimilation of precipitable water using a nonhydrostatic mesoscale adjoint model," Part I: Moisture retrieval and sensitivity experiments. *Mon. Wea. Rev.*, Vol.124, pp. 122-147, 1996. [https://doi.org/10.1175/1520-0493\(1996\)124<0122:VAOPWU>2.0.CO;2](https://doi.org/10.1175/1520-0493(1996)124<0122:VAOPWU>2.0.CO;2)
- [2] H. Seko, T. Kawabata, H. Nakamura, K. Koizumi, and T. Iwabuchi, "Impact of GPS-derived water vapor and radial wind measured by Doppler radar on numerical prediction of precipitation," *J. Meteor. Soc. Japan*, Vol.82, pp. 473-489, 2004. <http://doi.org/10.2151/jmsj.2004.473>
- [3] H. Nakamura, K. Koizumi, and N. Mannoji, "Data assimilation of GPS precipitable water into the JMA mesoscale numerical prediction model and its impact on rain fall forecast," *J. Meteor. Soc. Japan*, Vol.82, pp. 441-452, 2004. <http://doi.org/10.2151/jmsj.2004.441>
- [4] K. Koizumi and Y. Sato, "Impact of GPS and TMI precipitable water data on mesoscale numerical weather prediction model forecasts," *J. Meteor. Soc. Japan*, Vol.82, pp. 453-457, 2004. <http://doi.org/10.2151/jmsj.2004.453>
- [5] Y. Shoji, "A study of near real-time water vapor analysis using a nationwide dense GPS network of Japan," *J. Meteor. Soc. Japan*, Vol.87, pp. 1-18, 2009. <http://doi.org/10.2151/jmsj.87.1>
- [6] Y. Shoji, M. Kunii, and K. Saito, "Mesoscale data assimilation of Myanmar Cyclone Nargis. Part II: Assimilation of GPS-derived precipitable water vapor," *J. Meteor. Soc., Japan*, Vol.89, pp. 67-88, 2011. <http://doi.org/10.2151/jmsj.2011-105>
- [7] Y. Shoji, H. Yamauchi, W. Mashiko, and E. Sato, "Estimation of local-scale precipitable water vapor distribution around each GNSS station using slant path delay," *SOLA*, Vol.10, pp. 29-33, 2014. <http://doi.org/10.2151/sola.2014-007>
- [8] Y. Shoji, W. Mashiko, H. Yamauchi, and E. Sato, "Estimation of local-scale precipitable water vapor distribution around each GNSS station using slant path delay: Evaluation of a severe tornado case using high-resolution NHM," *SOLA*, Vol.11, pp. 31-35, 2015. <http://doi.org/10.2151/sola.2015-008>
- [9] T. Kawabata, Y. Shoji, H. Seko, and K. Saito, "A numerical study on a mesoscale convective system over a subtropical island with 4D-Var assimilation of GPS slant total delays," *J. Meteor. Soc., Japan*, Vol.91, pp. 705-721, 2013. <http://doi.org/10.2151/jmsj.2013-510>

- [10] H. Hatanaka, "Problems in near real-time GPS analysis," *Kisho-Kenkyu note*, Vol.192, pp. 145-158, 1998 (in Japanese).
- [11] H. Tsuji, "Principles of GPS, *Kisho-kenkyu note*," Vol.192, pp. 1-14, 1998 (in Japanese).
- [12] S. Shimada, S. Shimizu, and K. Tsuboki, "Impact of advanced ZTD estimation method – Separation from site coordinates estimation –," *Japan Geoscience Union Meeting*, May 24th-28th, Makuhari, Japan: Available from, 2015, [http://www2.jpgu.org/meeting/2015/session/PDF/M-TT05/ MTT05-02\\_E.pdf](http://www2.jpgu.org/meeting/2015/session/PDF/M-TT05/ MTT05-02_E.pdf) [accessed Sep. 18, 2017]
- [13] T. Washimi, "Report of heavy rainfall around Kani city on July 2010," *Natural Disaster Science*, Vol.29, No.2, pp. 259-267, 2010 (in Japanese).
- [14] Japan Meteorological Agency, "Heavy rainfall associated with Baiu front from 10 to 15 July, 2010," 2010, available from [http://www.data.jma.go.jp/obd/stats/data/bosai/report/2010/20100710/jyun\\_sokuji20100710-16.pdf](http://www.data.jma.go.jp/obd/stats/data/bosai/report/2010/20100710/jyun_sokuji20100710-16.pdf) [accessed Sep. 18, 2017]
- [15] M. Oue, K. Inagaki, T. Shinoda, T. Ohigashi, T. Kouketsu, M. Kato, K. Tsuboki, and H. Uyeda, "Polarimetric Doppler radar analysis of organization of a stationary rainband with changing orientations in July 2010.," *J. Meteor. Soc. Japan*, Vol.92, pp. 457-481, 2014, <http://doi.org/10.2151/jmsj.2014-503>
- [16] T. Herring, R. King, M.A. Floyd, and S.C. McClusky, "Introduction to GAMIT/GLOBK release 10.6," Massachusetts Institute of Technology, Cambridge, MA, 2015, available from [http://www.gpsg.mit.edu/~simon/gtgk/Intro\\_GG.pdf](http://www.gpsg.mit.edu/~simon/gtgk/Intro_GG.pdf) [accessed Sep. 18, 2017]
- [17] S. Shimada and K. Hioki, "Outline of GPS analysis," *Kisho-Kenkyu note*, Vol.192, pp. 61-72, 1998 (in Japanese).
- [18] K. Hioki, S. Shimada, and R. Ohtani, "GPS software," *Kisho-Kenkyu note*, Vol.192, pp. 73-92, 1998 (in Japanese).
- [19] R. Ohtani and I. Naito, "Physics in GPS precipitable water and its evaluation," *Kisho-Kenkyu note*, Vol.192, pp. 15-34, 1998 (in Japanese).
- [20] H. Nakagawa, T. Toyofuku, K. Kotani, B. Miyahara, C. Iwashita, S. Kawamoto, Y. Hatanaka, H. Munekane, M. Ishimoto, and T. Yutsudo, "GEONET new analysis strategy (version 4)," *J. Geogr. Surv. Inst.*, Vol.118, pp. 1-8, 2009 (in Japanese).
- [21] S. Shimizu and T. Maesaka, "Multiple Doppler radar analysis using variational technique to retrieve three-dimensional wind field," *Report of the National Research Institute for Earth Science and Disaster Prevention*, Vol.70, pp. 1-8, 2007 (in Japanese), [http://dil-opac.bosai.go.jp/publication/nied\\_report/PDF/70/70shimizu.pdf](http://dil-opac.bosai.go.jp/publication/nied_report/PDF/70/70shimizu.pdf) [accessed Sep. 18, 2017]
- [22] K. Shimose, S. Shimizu, T. Maesaka, R. Kato, K. Kieda, and K. Iwanami, "Impact of observation operators on low-level wind speed retrieved by variational multiple-Doppler analysis," *SOLA*, Vol.12, pp. 215-219, 2016, <http://doi.org/10.2151/sola.2016-043>
- [23] K. Tsuboki and A. Sakakibara, "Large-scale parallel computing of cloud resolving storm simulator," *High Performance computing*, Springer, H. P. Zima eds., pp. 243-259, 2002, [http://www.rain.hyarc.nagoya-u.ac.jp/~tsuboki/src/pdf\\_papers/ishpc2002\\_tsuboki.pdf](http://www.rain.hyarc.nagoya-u.ac.jp/~tsuboki/src/pdf_papers/ishpc2002_tsuboki.pdf) [accessed Sep. 18, 2017]
- [24] S. Shimizu, H. Uyeda, Q. Moteki, T. Maesaka, M. Takaya, K. Akaeda, T. Kato, and M. Yoshizaki, "Structure and formation mechanism on 24 May 2000 supercell-like storm developing in a moist environment over the Kanto Plain," *Mon. Wea. Rev.*, Vol.136, pp. 2389-2407, 2008, <https://doi.org/10.1175/2007MWR2155.1>
- [25] K. Saito, T. Fujita, Y. Yamada, J. Ishida, Y. Kumagai, K. Aranami, S. Ohmori, R. Nagasawa, S. Kumagai, C. Muroi, T. Kato, H. Eito, and Y. Yamazaki, "The operational JMA nonhydrostatic mesoscale model.," *Mon. Wea. Rev.*, Vol.134, pp. 1266-1298, 2006, <https://doi.org/10.1175/MWR3120.1>
- [26] Japan Meteorological Agency, "Outline of the operational numerical weather prediction at the Japan Meteorological Agency," *WMO Technical progress report on the global data-processing and forecasting system and numerical weather prediction*, 2007, available from <http://www.jma.go.jp/jma/eng/jma-center/nwp/outline-nwp/index.htm> [accessed Sep. 18, 2017]
- [27] Japan Meteorological Agency, "Outline of the operational numerical weather prediction at the Japan Meteorological Agency," *WMO Technical progress report on the global data-processing and forecasting system and numerical weather prediction*, 2013, available from <http://www.jma.go.jp/jma/eng/jma-center/nwp/outline2013-nwp/index.htm> [accessed Sep. 18, 2017]
- [28] Y. Kurihara, T. Sakurai, and T. Kuragano, "Global daily sea surface temperature analysis using data from satellite microwave radiometer," satellite infrared radiometer and in-situ observations. *Weather Bulletin*, JMA, Vol.73, pp. s1-s18, 2006 (in Japanese).
- [29] D. M. Barker, W. Huang, Y.-R. Guo, and Q. N. Xiao, "A three-dimensional variational data assimilation system for MM5: Implementation and initial results," *Mon. Wea. Rev.*, Vol.132, pp. 897-914, 2004, [https://doi.org/10.1175/1520-0493\(2004\)132<0897:ATVDAS>2.0.CO;2](https://doi.org/10.1175/1520-0493(2004)132<0897:ATVDAS>2.0.CO;2)
- [30] S. C. Bloom, L. L. Takacs, A. M. da Silva, and D. Ledvina, "Data assimilation using Incremental analysis updates.," *Mon. Wea. Rev.*, Vol.124, pp. 1256-1271, 1996, [https://doi.org/10.1175/1520-0493\(1996\)124<1256:DAUIAU>2.0.CO;2](https://doi.org/10.1175/1520-0493(1996)124<1256:DAUIAU>2.0.CO;2)
- [31] S. Shimizu, T. Kawabata, S. Yokota, H. Seko, M. Kunii, H. Yamauchi, K. Saito, Y. Shoji, S. Origuchi, D. Le, and K. Araki, "Development of data assimilation method," *Kisho-Kenkyu note*, chapter 5, pp. 1-5, 2017 (in print, in Japanese).
- [32] J. T. Stauffer and N. L. Seaman, "Multiscale four-dimensional data assimilation," *J. Appl. Meteor.*, Vol.33, pp. 416-434, 1994, [https://doi.org/10.1175/1520-0450\(1994\)033<0416:MFDDA>2.0.CO;2](https://doi.org/10.1175/1520-0450(1994)033<0416:MFDDA>2.0.CO;2)
- [33] Y. Ishikawa, "Use of ground-base GPS data for mesoscale analysis, Report of numerical," *Annual report of the Numerical Prediction Division of JMA*, Vol.56, pp. 56-60, 2011 (in Japanese).



**Name:**  
Shingo Shimizu

**Affiliation:**  
Senior Researcher, Storm, Flood and Land-slide Research Division, National Research Institute For Earth Science and Disaster Resilience (NIED)

**Address:**  
3-1 Tennodai, Tsukuba, Ibaraki 305-0006, Japan

**Brief Career:**  
2006- Associate Research Fellow, NIED  
2008- Researcher with Tenure, NIED  
2012- Senior Researcher, NIED

**Selected Publications:**

- "Algorithm for the identification and tracking convective cells based on constant and adaptive threshold methods using a new cell-merging and -splitting scheme," *J. Meteor. Soc. Japan*, Vol.90, pp. 868-889, 2012.
- "Structure and formation mechanism of a 24 May 2000 supercell-like storm developing in a moist environment over Kanto Plain," *Japan. Mon. Wea. Rev.* Vol.136, pp. 2389-2407, 2007.
- "Multiple Doppler radar analysis for retrieving the three-dimensional wind field within thunderstorm," S. Shimizu, InTech Press, Chapter 9 in "Doppler radar observations," ISBN 978-953-51-0496-4, p. 482, 2012.

**Academic Societies & Scientific Organizations:**

- Meteorological Society of Japan (MSJ)



**Name:**  
Seiichi Shimada

**Affiliation:**  
Project Researcher, Department of Environment  
Systems, Graduate School of Frontier Sciences,  
The University of Tokyo

**Address:**

5-1-1 Kashiwanoha, Kashiwa, Chiba 277-8563, Japan

**Brief Career:**

1979-2015 National Research Institute For Earth Science and Disaster  
Resilience (NIED)  
2015- The University of Tokyo

**Selected Publications:**

- "A small persistent locked area associated with the 2011 Mw9.0 Tohoku-Oki earthquake, deduced from GPS data," J. of Geophysical Research, Vol.117, B11408, 2012.
- "Comparison of the coordinates solutions between the absolute and the relative phase center variation models in the dense regional GPS network in Japan," Geodesy for Planet Earth, pp. 651-656, 2012.
- "The impact of atmospheric mountain lee waves on systematic geodetic errors observed using the Global Positioning System," Earth Planets Space, Vol.54, pp. 425-430, 2002.

**Academic Societies & Scientific Organizations:**

- Geodetic Society of Japan (GSJ)
  - American Geophysical Union (AGU)
- 



**Name:**  
Kazuhisa Tsuboki

**Affiliation:**  
Professor, Institute for Space-Earth Environmen-  
tal Research (ISEE), Nagoya University

**Address:**

Furo-cho, Chikusa-ku, Nagoya, Aichi 464-8601, Japan

**Brief Career:**

2001-2012 Associate Professor of Hydrospheric Atmospheric Research  
Center (HyARC), Nagoya University  
2012-2015 Professor of, HyARC Nagoya University  
2015-present Professor of ISEE, Nagoya University

**Selected Publications:**

- K. Tsuboki and A. Sakakibara, "Large-Scale parallel computing of cloud resolving storm simulator," High Performance Computing Spring, pp. 243-259, 2002.
- K. Tsuboki, "Westward movement and splitting of equatorial cloud cluster associated with tropical large-scale vortices," J. of Meteorological Society, Japan, Vol.75, pp. 23-42, 1997.
- K. Tsuboki and G. Wakahama, "Mesoscale cyclogenesis in winter monsoon air streams: Quasi-geostrophic baroclinic instability as a mechanism of the cyclogenesis off the west coast of Hokkaido island," Japan, J. of Meteorological Society, Japan, Vol.70, pp. 267-290, 1992.

**Academic Societies & Scientific Organizations:**

- Meteorological Society of Japan (MSJ)
  - Japan Society of Hydrology and Water Resources (JSHWR)
  - Japan Society for Natural Disaster Science (JSNDS)
-